DOI: 10.1002/ ((please add manuscript number))
Article type: Full Paper

Photo-Induced Absorption Spectroscopy of CoPi on $BiVO_4$: The Function of CoPi During Water Oxidation

*Yimeng Ma, Andreas Kafizas, Stephanie R. Pendlebury, Florian Le Formal and James R. Durrant**

Dr. Yimeng Ma, Dr. Andreas Kafizas, Dr. Stephanie R. Pendlebury, Dr. Florian Le Formal, Prof. James R. Durrant
Department of Chemistry, Imperial College London, South Kensington Campus, Exhibition Road, London, SW7 2AZ, United Kingdom
E-mail: j.durrant@imperial.ac.uk

Dr. Andreas Kafizas
Christopher Ingold Laboratories, Department of Chemistry, University College London, Gordon Street, London, WC1H 0AJ, United Kingdom

Dr. Florian Le Formal
Laboratory for Molecular Engineering of Optoelectronic Nanomaterials, Institute of Chemical Sciences and Engineering, École Polytechnique Fédérale de Lausanne (EPFL), Station 6, Lausanne 1015, Switzerland

Keywords: cobalt phosphate, bismuth vanadate, water oxidation, photoelectrochemistry, kinetics

In this paper, we employ photoinduced absorption and electrochemical techniques to analyze the charge carrier dynamics that drive photoelectrochemical water oxidation on $BiVO_4$, both with and without CoPi co-catalyst. These results are correlated with spectroelectrochemical measurements of Co^{II} oxidation to Co^{III} in a CoPi/FTO electrode during dark electrocatalytic water oxidation. Electrocatalytic water oxidation exhibits a non-linear dependence on Co^{III} density, with a sharp onset at 1 x 10^{17} Co^{III} cm^{-2}. These results are compared quantitatively with the degree of CoPi oxidation observed under conditions of photo-induced water oxidation on CoPi-$BiVO_4$ photoanodes. For the CoPi-$BiVO_4$ photoanodes studied herein, ≤ 5 % of water oxidation proceeds from CoPi sites, making the $BiVO_4$ surface the predominant water oxidation site. This study highlights two key factors that limit the ability of CoPi to improve the catalytic performance of $BiVO_4$: 1) the kinetics of hole transfer from the $BiVO_4$ to the CoPi layer are too slow to effectively compete with direct water oxidation from $BiVO_4$;

2) the slow water oxidation kinetics of CoPi result in a large accumulation of Co^{III} states, causing an increase in recombination. Addressing these factors will be essential for improving the performance of CoPi on photoanodes for solar-driven water oxidation.

1. Introduction

Photoelectrochemical (PEC) water splitting has the potential to be an effective method to generate hydrogen as a renewable fuel.[1] The overall process consists of two half reactions: proton reduction to produce hydrogen and water oxidation to generate oxygen. The water oxidation, typically driven on n-type photoanodes, is kinetically more difficult as four oxidizing equivalents (holes) are required to generate one oxygen molecule.[2] As such, one widely used strategy to enhance water oxidation function is to modify the surface of the semiconductor photoanode with electrocatalysts. This approach has been shown to increase PEC water oxidation efficiency by both decreasing the photocurrent onset potential and increasing the photocurrent density.[3] Most studies have attributed this enhancement to hole transfer from the semiconductor to the catalyst,[3b, 4] with water oxidation proceeding from the electrocatalyst surface. However, other studies have suggested that such electrocatalyst surface modification can also reduce recombination losses in the photoanode, and indeed suggested that this can be, for some systems, the primary cause of the improved water splitting performance.[2b, 5] Such arguments depend in part on the relative kinetics of water oxidation on the semiconductor and electrocatalyst surface; in other words, the extent to which the semiconductor exhibits faster water oxidation kinetics than the electrocatalyst itself. In the study reported herein, we address this issue for one such system: cobalt phosphate (CoPi) modified bismuth vanadate ($BiVO_4$) photoanodes. We have previously reported that CoPi deposition on $BiVO_4$ can retard recombination losses in this photoanode.[5e] Herein, we employ quasi steady-state photo-induced absorption analyses to quantify hole accumulation and water oxidation on both the electrocatalyst and semiconductor, and thereby develop a full

kinetic model of the photoanode function. We come to the striking conclusion that whilst photo-irradiation results in substantial hole accumulation on CoPi, the kinetics of water oxidation on the semiconductor are actually faster than on the electrocatalyst. For our photoanodes, over 95% of water oxidation proceeds directly from the $BiVO_4$ surface.

Cobalt phosphate (CoPi) is an efficient water oxidation electrocatalyst first reported by Kanan and Nocera.[6] Water oxidation is catalyzed by CoPi *via* oxidation of Co^{II} to Co^{IV}, with these oxidations proceeding by proton-coupled electron transfer (PCET). The PCET process has been proposed as the rate limiting step for water oxidation on CoPi electrodes.[7] Whilst the turnover frequency per catalytic site is relatively low ($0.01 – 0.001\ s^{-1}$),[7-8] , CoPi is capable of oxidizing water with a low overpotential and high current densities due to its high internal surface area.

Depositing CoPi on n-type photoanodes has resulted in significant increase in water oxidation photocurrent densities and cathodically shifted onset potentials. Typical examples are CoPi-modified $BiVO_4$[3b, 3c, 9] and hematite (α-Fe_2O_3)[4a, 10] photoanodes. We have previously reported transient absorption (employing 6 ns pulsed laser excitation) and transient photocurrent (with white light bias) studies of CoPi-modified α-Fe_2O_3 and undoped $BiVO_4$ photoanodes.[5c-f] These optical techniques directly monitor the dynamics of the photo-induced holes responsible for water oxidation, and demonstrated that CoPi modification suppresses 'back electron/hole' or 'surface' recombination, i.e. electron transfer from the semiconductor bulk to surface accumulated holes. Thus, whilst CoPi oxidation was observed under anodic potentials,[5c-f] the results suggested a suppression of recombination losses within the semiconductor was the primary origin of the cathodic shift in photocurrent onset potential and the increased photocurrent density.[5e] In contrast, impedance spectroscopy[4a, 11] and PEC[3b, 10a] studies of CoPi-modified α-Fe_2O_3 photoanodes under continuous illumination have suggested that water oxidation occurs *via* a hole transfer process to CoPi, which then catalyzes the water oxidation reaction. The study reported herein aims to address this

controversy by quantifying the degree of oxidation of the CoPi catalyst on a $BiVO_4$ photoanode under irradiation, and determining whether this degree of catalyst oxidation is sufficient to drive significant water oxidation.

A key issue regarding the function of electrocatalyst-modified photoanodes is to quantify the relative kinetics of water oxidation on the semiconductor and electrocatalyst surfaces. A key figure of merit for electrocatalysts is their ability to drive reactions at low overpotentials. In contrast, most metal oxide based photoanodes exhibit deep valence band energies, such that valence band holes possess a large driving force for water oxidation. Rate constants for water oxidation on such photoanodes are on the order of 1-10 s^{-1},[2, 5a, 5b, 12] comparable to or faster than rate constants per catalytic site for most water oxidation electrocatalysts.[13] (We note that electrocatalytic rate constants are typically quoted in per unit areas , complicating a direct comparison.) In this regard, it does not immediately follow that a surface electrocatalyst will accelerate water oxidation. A further consideration is the permeability of electrocatalysts to water, such that even following electrocatalyst deposition, water oxidation can still proceed directly from the semiconductor surface. As such, the relative kinetics of hole transfer from the semiconductor to the electrocatalyst *versus* direct transfer to water (*i.e.* water oxidation) may also play a key role in the function of a modified photoanode. Neither of these issues – the relative kinetics of water oxidation on the semiconductor and electrocatalyst surfaces, and the kinetics of hole transfer to electrocatalyst *versus* water oxidation – have received significant attention in the literature to date, and are the specific focus of this study.

In this study, photo-induced absorption (PIA) spectroscopy was employed to investigate the kinetics of photo-induced species in $BiVO_4$ and CoPi-modified $BiVO_4$ photoanodes under long-pulse (several seconds) illumination. The photocurrent response was monitored concurrently, thus allowing the steady-state electron and hole dynamics to be obtained simultaneously. Spectroelectrochemical (SEC) measurements of CoPi/FTO electrodes were also conducted for the study of electrocatalytic water oxidation on CoPi. The function of CoPi

on $BiVO_4$ photoanodes is elucidated by comparing the behavior during electrocatalytic water oxidation in the dark and photoelectrochemical water oxidation under illumination.

2. Results

2.1. Physical and Photoelectrochemical Characterization

We have previously reported our synthesis for depositing CoPi on a 450 nm thick $BiVO_4$ photoanodes, which yields an approximately 100 nm thick CoPi layer.[5e] The thickness of CoPi grown directly onto FTO was also ~100 nm (see SEM images in **Figure S1** in the Supporting Information). XPS analysis of CoPi/$BiVO_4$/FTO films confirmed the presence of Co, P, Bi, V and O, alongside adventitious carbonaceous residues typically found on materials handled in air (C, Si and O). **Figure 1** shows both the Co 2p and 3p environments and their deconvoluted constituents. The Co $2p_{3/2}$, $2p_{1/2}$ and 3p binding energies are centered at 781.5, 796.8 and 62.5 eV respectively. These results indicate the presence of both Co^{II} and/ or Co^{III} oxidation states in environments similar to $Co(OH)_2$ and Co_2O_3 respectively,[14] and has been previously attributed to the formation of a mixed Co^{II} and Co^{III} phosphate.[6] This is consistent with a recent report of CoPi-modified Fe_2O_3 photoanodes,[15] as well as analyses of CoPi electrocatalysts.[7] Similar behavior was observed in CoPi grown directly on FTO (see Supporting Information **Figure S2**). XPS analysis also revealed a near 1:1 ratio of Bi^{3+} ($4f_{7/2}$ = 159.1 eV)[16] and V^{5+} ($2p_{3/2}$ = 516.6 eV),[17] as expected for $BiVO_4$ (see Supporting Information **Figure S3**). It is noteworthy that for the CoPi-modified electrode, $BiVO_4$ was observed (albeit in a much lower concentration than CoPi) even without sputtering. As XPS is a highly surface-sensitive technique, where only photoelectron emissions from the first ~10 nm of material are normally detected,[18] this indicates a non-uniform coverage of $BiVO_4$ by CoPi. This result is consistent with SEM images that reveal cracks between isolated CoPi domains (see Supporting Information and previous literature[5e]). XRD indicates that the deposited CoPi overlayers on both $BiVO_4$ and FTO are amorphous (Supporting Information

Figure S1c), consistent with previous literature.[5e, 6] The $BiVO_4$ layers are crystalline, adopting the clinobisvanite structure (a = 5.177(8), b = 5.106(7), c = 11.69(1); wRp = 0.106), with crystallites on average 60–70 nm wide.

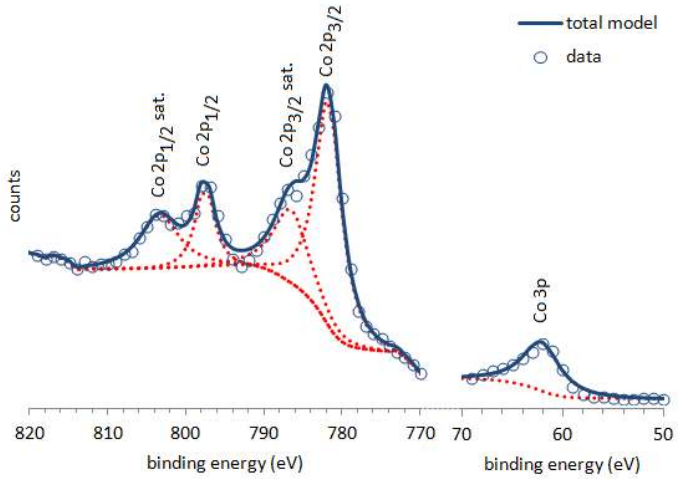

Figure 1. XPS analysis of CoPi-modified $BiVO_4$ showing the Co_{2p} (820 – 770 eV) and Co_{3p} (70 – 50 eV) binding energy regions and the deconvolution of each Co state and satellite states.

Figure 2a shows the cyclic voltammetry (CV) of $BiVO_4$ and CoPi-modified $BiVO_4$ in the dark (dotted lines) and under 365 nm continuous LED illumination (solid lines). It is apparent that the CoPi overlayer enhances the photoelectrochemical performance of $BiVO_4$ both in terms of a cathodic shift of onset potential (by 400 mV) and an increase in photocurrent density (by a factor of two), consistent with previous reports.[3b, 5e, 9a] In addition, the dark onset potential was also cathodically shifted by 250 mV after CoPi deposition, due to CoPi electrocatalytic water oxidation on $BiVO_4$, consistent with the dark electrocatalytic activity of CoPi on FTO (**Figure 2b**).

A shoulder in the CV trace of CoPi-modified $BiVO_4$ in the dark is observed at ~1.65 V_{RHE} (**Figure 2a**), consistent with a previous report.[5e] A similar reversible redox wave is observed for CoPi/FTO at 1.55 V_{RHE} (**Figure 2b**), in agreement with previous reports of CoPi

electrochemical oxidation/reduction.[6, 8] The small anodic shift (~100 mV) in this oxidation wave of CoPi on $BiVO_4$ compared to CoPi on FTO is attributed to resistance losses in $BiVO_4$. At more anodic applied potentials, the CoPi/FTO current increases rapidly with increasing applied potential, assigned as previously to electrocatalytic water oxidation. The amplitude of the shoulder at 1.55 V_{RHE} on CoPi/FTO decreases with decreasing scan rate, disappearing entirely under steady-state conditions (see Supporting Information **Figure S4**). This demonstrates that the shoulder at 1.55 V_{RHE} for CoPi/FTO (and at 1.65 V_{RHE} for CoPi-modified $BiVO_4$) is due to a charging process rather than a Faradaic current. As such, the shoulder at 1.65 V_{RHE} in the CoPi/$BiVO_4$ CV is attributed to CoPi oxidation, specifically the oxidation of Co^{II} to Co^{III},[6-7] as supported by the XPS results discussed above.

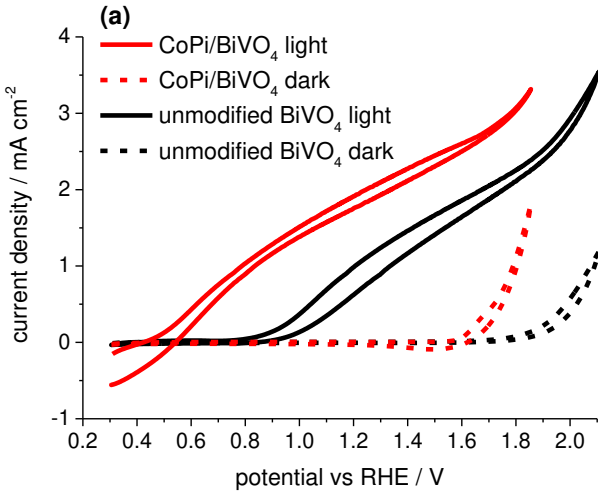

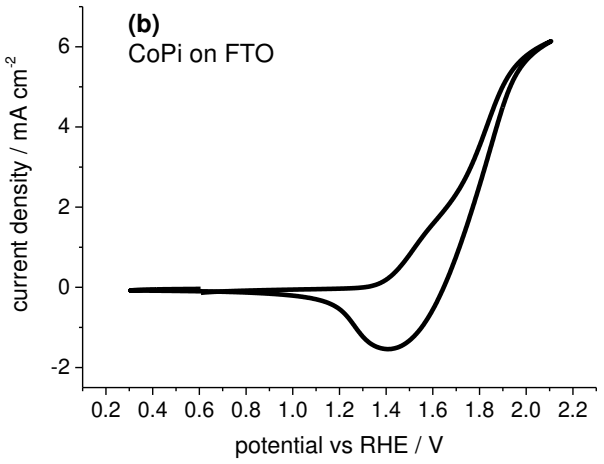

Figure 2. (a) Cyclic voltammetry measurements (in KPi buffer, pH 6.7) of CoPi-modified $BiVO_4$ (red) and unmodified $BiVO_4$ (black) measured under 365 nm illumination (equivalent to 100% AM1.5; solid lines) and in the dark (dotted lines). (b) CV measurement of a CoPi/FTO electrode in KPi buffer, in the dark. Scan rate: 100 mV s^{-1}.

2.2. Photo-Induced Absorption Spectroscopic Study

The photo-induced species in unmodified and CoPi-modified $BiVO_4$ were monitored under quasi steady-state conditions by photo-induced absorption spectroscopy (referred as 'PIA' spectroscopy). This technique is similar to the pump-probe transient absorption spectroscopy (TAS) previously employed by ourselves[5e, 12b-e, 12g] and others[19] to investigate charge carrier dynamics in water splitting photoelectrodes. However, in contrast to TAS, our PIA technique employs long (several seconds) light pulses to excite the sample. This allows us to investigate the change in photo-generated charge carrier density as a function of light intensity under quasi steady-state working conditions.[20]

Figure 3 shows the simultaneously measured PIA at 550 nm (a) and photocurrent (b) as a function of time for $BiVO_4$ and CoPi-modified $BiVO_4$ at potentials of at 1.7 V_{RHE} and 1.4 V_{RHE} respectively (as these potentials lie just cathodic of the dark water oxidation onset potential), and an 365 nm LED excitation intensity equivalent to 87 % of AM 1.5 in terms of photon flux (see Supporting Information). The corresponding PIA spectra are shown in **Figure 3c**.

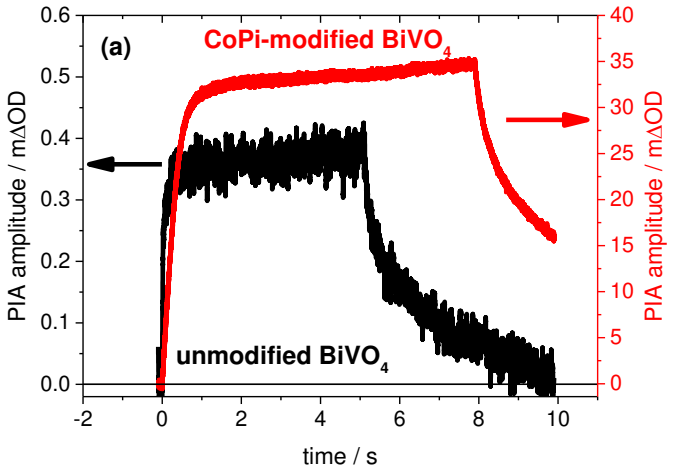
(a)
CoPi-modified BiVO4
unmodified BiVO4
PIA amplitude / mΔOD
PIA amplitude / mΔOD
time / s
0.6
0.5
0.4
0.3
0.2
0.1
0.0
40
35
30
25
20
15
10
5
0
-2
0
2
4
6
8
10

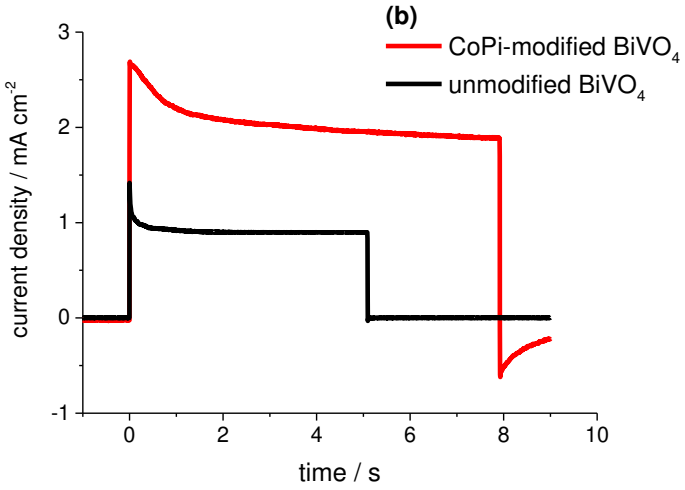
(b)
CoPi-modified BiVO4
unmodified BiVO4
current density / mA cm-2
time / s
3
2
1
0
-1
0
2
4
6
8
10

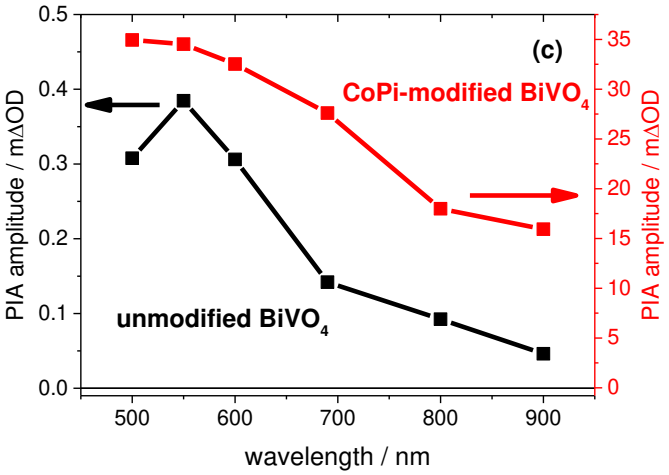

Figure 3. (a) PIA response of the unmodified (black, under 1.7 V_{RHE}) and CoPi-modified (red, under 1.4 V_{RHE}) $BiVO_4$ photoanode. The probe wavelength is 550 nm; the excitation wavelength is 365 nm (excitation intensity: 87 % of AM 1.5). Length of excitation pulse: 5 s for unmodified $BiVO_4$ and 8 s for CoPi-modified $BiVO_4$. (b) Photocurrent response measured at the same time as PIA measurements. (c) PIA spectra of the unmodified and CoPi-modified $BiVO_4$.

We will first consider the PIA data of unmodified $BiVO_4$. The PIA spectrum of unmodified $BiVO_4$ at strong positive potential (1.7 V_{RHE}) exhibits a broad absorption from the visible to the near-IR, with a peak at 550 nm (**Figure 3c**). This PIA spectrum is in good agreement with the transient absorption spectra of long-lived photogenerated holes in $BiVO_4$, previously observed using electron scavengers and applied anodic potentials.[12c] Therefore the PIA signal from unmodified $BiVO_4$ photoanodes is assigned to long-lived, surface accumulated $BiVO_4$ holes. Of note, the shape of this PIA spectrum did not change with light intensity (Supporting Information **Figure S5**), which was a strong indication that the chemical nature of these accumulated holes is independent of the excitation pulse intensity and length.

Previous transient absorption studies have shown that bulk recombination in $BiVO_4$ occurs on the picosecond to microsecond timescales,[5e, 12c, 19a] while water oxidation and the

recombination of surface-accumulated holes with bulk electrons occurs on the millisecond to second timescales, corresponding to the timescales probed in the experiments reported herein (the PIA time resolution is 0.4 ms).[12c, 20] At the strong anodic potential employed in **Figure 3** (1.7 V_{RHE}), back electron/hole recombination is largely suppressed.[2b, 5a, 5e, 5f, 12a, 12b] Thus, the PIA kinetics of unmodified $BiVO_4$ shown in **Figure 3a** primarily probe the accumulation of long-lived holes at the surface of the photoanode and their consumption *via* water oxidation. (Previous photoelectrochemical studies of unmodified $BiVO_4$ photoanodes have reported near unit faradaic efficiencies for water oxidation and oxygen evolution.[21]) The positive rise of PIA signals from unmodified $BiVO_4$ is attributed to hole accumulation resulting from the photo-induced hole flux towards the surface, as described previously for α-Fe_2O_3 photoanodes.[20] The plateauing of the PIA signal after ~1 s of light exposure is indicative of this hole flux towards the $BiVO_4$ surface reaching an equilibrium with the flux of holes transferring to the electrolyte (water oxidation), as detailed previously for the PIA study of α-Fe_2O_3 photoanodes.[20] When the light is turned off, the flux of holes to the surface ceases and the decaying PIA signal is assigned to the consumption of these surface accumulated holes by water oxidation.

The transient photocurrent (TPC) data were recorded simultaneously with the PIA measurements**. Figure 3b** compares the TPC of unmodified (black) and CoPi-modified (red) $BiVO_4$ photoanodes under strong anodic potentials. For the unmodified $BiVO_4$, the rapid decay of the photocurrent within ~1 s of light-on is due to an increase in electron/hole recombination (bulk and/or surface) losses. We attribute this to reduced band bending as photogenerated holes accumulate at the surface.[20] After light-off, the current returns to zero within the time resolution of the measurement (< 0.4 ms). This is in contrast with the optical signals, which decay much more slowly ($t_{50\%}$ of the decay from the steady state after light off is ~0.5 s). Following CoPi modification, photocurrent densities were approximately two fold larger, assigned to reduced recombination losses (see discussion below).[5c, 5e] The negative

current transient of CoPi-modified $BiVO_4$ shown in **Figure 3b** suggests that there is significant back electron/hole recombination after light off, which this was not observed for the unmodified $BiVO_4$.

As we have reported previously for Fe_2O_3, the extinction coefficient of photogenerated surface holes can be determined by comparing the amplitudes of the PIA and TPC at applied potentials close to the photocurrent onset, where back electron/hole recombination dominates over water oxidation. This analysis was undertaken for the unmodified $BiVO_4$, as detailed in the supporting information (**Figure S6**), leading to a $BiVO_4$ molar extinction coefficient at 550 nm of 420 ± 20 M^{-1} cm^{-1}. Employing this value, from **Figure 3a**, we obtain a surface hole density of ~4 x 10^{14} cm^{-2} at the steady state of PIA measurements under the strong anodic bias conditions used for these studies.

We now consider the PIA for the CoPi-modified $BiVO_4$, as shown in **Figure 3a** and **3c**. It is apparent that the PIA signals for the CoPi-modified $BiVO_4$ are approximately one hundred times greater than that of the unmodified $BiVO_4$ (note the different PIA y-axis scales used for the unmodified and CoPi-modified $BiVO_4$). This large difference in signal amplitude is in striking contrast to the difference in photocurrent density, where CoPi deposition results in only approximately two times greater photocurrent density (**Figure 3b**). It is also apparent that the PIA spectrum of CoPi-modified $BiVO_4$ (red line and squares in **Figure 3c**) is significantly broader than for unmodified $BiVO_4$ (black line and squares in **Figure 3c**). This suggests that that the significantly larger PIA signal observed in CoPi-modified $BiVO_4$ is due to an *additional* photo-induced species, rather than photogenerated holes in $BiVO_4$. As we discuss below, comparison with spectroelectrochemical data for CoPi/FTO, allows us to assign the large PIA signal observed for CoPi-modified $BiVO_4$ primarily to CoPi oxidation.

2.3. Spectroelectrochemical Measurements of CoPi on FTO

We turn now to spectroelectrochemical (SEC) analysis of dark electrocatalytic water oxidation by CoPi on FTO. The CoPi layer is of comparable thickness to the CoPi overlayers employed on $BiVO_4$, i.e. ~100 nm. SEC absorption difference spectra were obtained by subtracting the steady-state absorption spectrum, measured without applied potential (at open circuit), from the steady-state absorption spectra under applied potential. The anodic current onset for CoPi/FTO is at 1.4 V_{RHE} at a scan rate of 100 mV s^{-1} (**Figure 2c**). **Figure 4a** presents the SEC results of CoPi/FTO as a function of anodic potential from 1.4 to 2.4 V_{RHE}. For each measurement, the potential was applied for 60 s before the UV-visible absorption spectrum was collected. The positive change in SEC absorbance (mΔOD) is assigned to additional absorption from oxidized CoPi species generated by the positive applied potential. The spectra, obtained from 500 nm to 900 nm, are of similar shape across the potential range employed, characterized by a broad absorption that decreases towards longer wavelengths. This indicates that the same oxidized species is observed from 1.4 to 2.4 V_{RHE} for CoPi/FTO. XPS analyses (see Supporting Information) indicate that the oxidation state of cobalt in CoPi/FTO is primarily 2+, in agreement with previous reports[6-7] and with our analyses of CoPi-modified $BiVO_4$ discussed above. Therefore we assign the SEC absorption increase occurring at potentials anodic of 1.4 V_{RHE} to the oxidation of Co^{II} to Co^{III}. This assignment is also supported by literature studies reporting stronger visible light absorption for Co^{III}[13] compared to Co^{II}.[21]

By correlating the optical absorption and the charging current (Co^{II} to Co^{III}) of CoPi/FTO between 1.4 V_{RHE} and 1.6 V_{RHE}, the extinction coefficient of the Co^{III} species observed in our SEC data was calculated to be ~620 ± 60 M^{-1} cm^{-1} at 550 nm (see **Figure S7** in Supporting Information). This allows the density of Co^{III} species to be determined as a function of anodic potential, as plotted in **Figure 4b**. It is apparent that this density increases from 6×10^{15} (1.4 V_{RHE}) up to 1.4×10^{17} (2.0 V_{RHE}) Co^{III} cm^{-2} at strong anodic potential. We note that the increased absorption corresponds to the additional Co^{III} species generated by the applied

potential. The potential-dependent Co^{III} density is overlaid upon the corresponding dark cyclic voltammetry data measured at a fast scan speed (100 mV s^{-1}, red dashed line) and the steady state current *versus* applied potential (red solid lines with squares) in **Figure 4b**. The saturated currents measured anodic of 2.0 V_{RHE} are likely to be limited by the mass transport of O_2 from the CoPi into the electrolyte.[7] As discussed above, the shoulder in the fast CV scan at ~1.55 V_{RHE} is assigned to oxidation of Co^{II} to Co^{III}. The onset of the steady state current occurs at 1.7 V_{RHE}, assigned to electrocatalytic water oxidation. This difference between the shoulder and the steady-state current onset is assigned to the requirement for the further oxidation of Co^{III} to Co^{IV} for significant water oxidation to occur, in agreement with literature reports.[7, 22] It is striking that the spectroelectrochemical absorption onset is at the same potential as the Co^{II} to Co^{III} oxidation wave, which is ~300 mV cathodic of the onset of water oxidation.

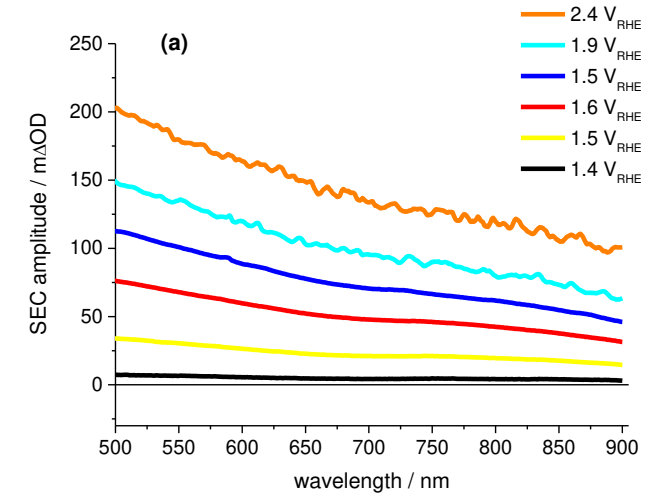

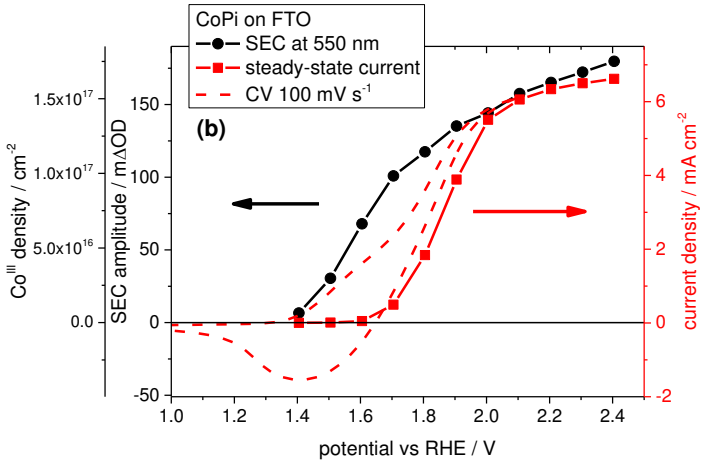

Figure 4. (a) Spectroelectrochemical difference spectra of CoPi/FTO measured as a function of applied potential from 1.4 V_{RHE} to 2.4 V_{RHE}. All difference spectra are generated by subtracting by the spectrum measured at open-circuit from the spectrum measured under applied potential. (b) The amplitude of the CoPi/FTO spectra at 550 nm and calculated Co^{III} density (cm^{-2}) as a function of applied potential (solid black line and circles); the steady-state current recorded during SEC measurements of CoPi/FTO (solid red line and squares); CV measurement of CoPi/FTO as a function of applied potential with a scan rate of 100 mV s^{-1} (dashed red lines).

The spectroelectrochemical absorption increases for CoPi/FTO observed from 1.4 V_{RHE} to 2.4 V_{RHE} as shown in **Figure 4a** are rather large (up to 0.2 ΔOD). They are larger, except at very modest anodic potentials, than the absorption increases observed in the photo-induced absorption studies of CoPi-modified $BiVO_4$ (discussed above). In particular, at the onset of electrochemical water oxidation (1.7 V_{RHE}), the SEC absorption signal at 550 nm is ~110 mΔOD (corresponding to 1×10^{17} Co^{III} cm^{-2}). This is a three-fold higher signal than that observed in our PIA measurements of CoPi-modified $BiVO_4$ (35 mΔOD, corresponding to 3.2×10^{16} Co^{III} cm^{-2} from **Figure 3a**) under our conditions of photoelectrochemical water oxidation. As such, we conclude that the density of Co^{III} species on CoPi/$BiVO_4$ under conditions of photoelectrochemical water oxidation is *ca.* three fold lower than that observed on CoPi/FTO at the onset of dark electrochemical water oxidation. The significance of this observation for the mechanism of photoelectrochemical water oxidation is discussed in detail below.

3. Discussion

In the study reported herein, we have used optical spectroscopic methods to probe the photogenerated species generated on CoPi-modified $BiVO_4$ photoanodes under steady-state water oxidation conditions. Photo-induced absorption spectroscopy allows photogenerated

charge carrier densities to be monitored directly under the working conditions of photoelectrochemical water oxidation, *i.e*. under continuous wave excitation and external applied potentials. We assign the visible-near IR (500-900 nm) photo-induced absorption (PIA) spectrum of unmodified $BiVO_4$ to photogenerated holes at the photoanode surface. The PIA amplitude is two orders of magnitude greater for CoPi-modified $BiVO_4$ than for unmodified $BiVO_4$, under the same excitation conditions. In contrast, the photocurrent is increased only two fold by CoPi deposition. Furthermore, the PIA spectra for CoPi-modified $BiVO_4$ is distinct from that of $BiVO_4$, but similar to that observed for the dark electrochemical oxidization of a CoPi/FTO electrode. It is thus concluded that the photoinduced absorption signal observed for CoPi-modified $BiVO_4$ photoanodes under irradiation at anodic bias is primarily due to the accumulation of oxidized CoPi, specifically Co^{III} species, due to the oxidation of CoPi by photogenerated holes in $BiVO_4$.

The comparison of these optical absorption signals (monitoring surface-accumulated positive charges) and photocurrent (monitoring electrons extracted to the external circuit) is now considered. Water oxidation in natural and artificial photosynthesis requires the accumulation of positive charges.[2a] Previous transient absorption,[12c] and these PIA studies, of unmodified $BiVO_4$ have demonstrated that the accumulation of long-lived (milliseconds to seconds lifetime) holes at the photoanode surface is required for water oxidation.

In the CoPi-modified $BiVO_4$ system, the significantly increased absorption signal (two orders of magnitude greater than unmodified $BiVO_4$) is assigned to the accumulation of Co^{III} species within the CoPi layer. CoPi oxidation under irradiation of CoPi-modified photoanodes has also been reported previously by other groups.[3b, 4a, 10a, 11] However this observation alone does not prove that the photoelectrochemical water oxidation current derives from this CoPi oxidation. Using our measured extinction coefficient at 550 nm for Co^{III} states in CoPi, we estimate that under our conditions of photoelectrochemical water oxidation on CoPi-$BiVO_4$ (1.7 V_{RHE} and 2 mA cm^{-2}), the density of Co^{III} species is 3.2×10^{16} cm^{-2}. To evaluate whether

this degree of oxidation of the CoPi layer is sufficient to drive the 2 mA cm^{-2} of water oxidation photocurrent density observed under irradiation, we used a spectroelectrochemical (SEC) analysis of electrochemical water oxidation on CoPi/FTO, employing a similar CoPi deposition route and thickness to that used in our CoPi-modified $BiVO_4$ photoanodes (see **Figure 4**). **Figure 5a** summarizes the conclusion of this study, showing the steady-state electrochemical water oxidation current from CoPi/FTO as a function of density of Co^{III} species. It is apparent that the water oxidation current does not increase linearly with increasing Co^{III} concentration. Rather, the electrochemical water oxidation current exhibits on onset at ~1×10^{17} Co^{III} cm^{-2} (110 mΔOD), approximately 1 % of total cobalt density (8.6×10^{18} cm^{-2}) in a 100 nm thick film. The current density increases rapidly with increasing anodic potential, before saturating at ~ 7 mA cm^{-2}, most probably due to electrolyte mass transport limitations. This photocurrent onset behavior as a function of Co^{III} density is assigned to the requirement for the further oxidation of Co^{III} to Co^{IV} to enable water oxidation, as indicated in several literature reports.[7, 22] It is apparent that this Co^{III} to Co^{IV} oxidation only occurs once the density of Co^{III} species in the CoPi exceeds 1×10^{17} cm^{-2}.

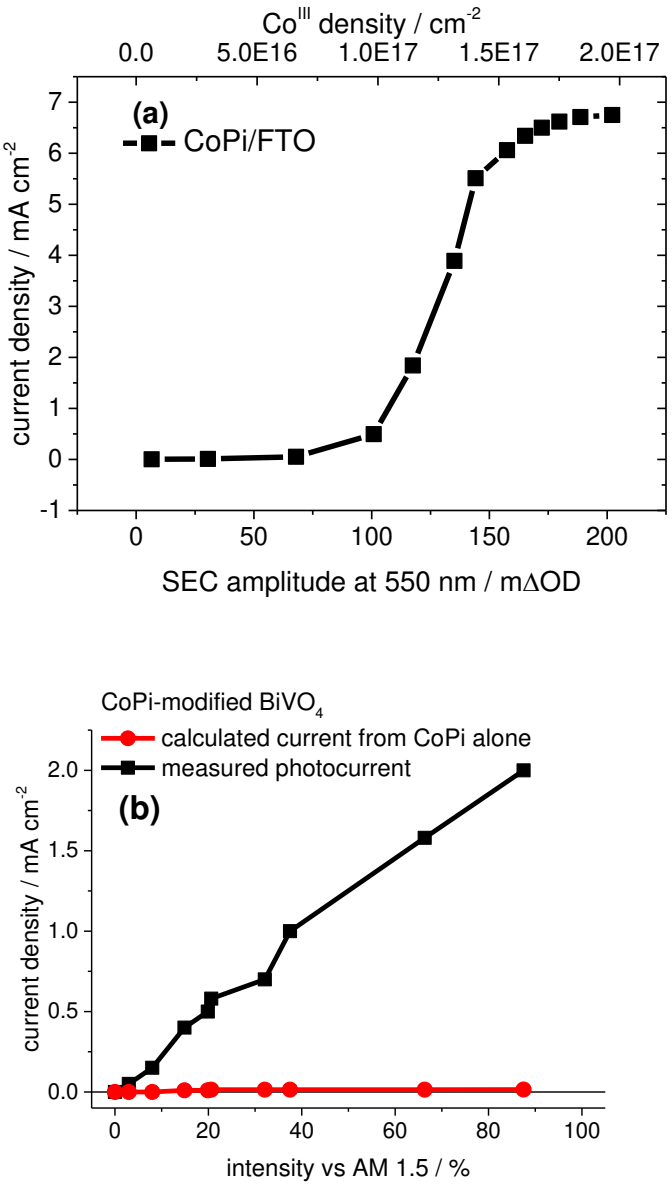

Figure 5. (a) Steady-state photocurrent density measured during spectroelectrochemistry (SEC), as a function of the absorbance at 550 nm in the SEC difference spectra for CoPi/FTO (data from **Figure 4b**). (b) Black: photocurrent of CoPi-modified $BiVO_4$ measured during PIA, as a function of excitation light intensity; red: calculated photocurrent from CoPi-modified $BiVO_4$, assuming water oxidation proceeds from CoPi alone, and that the PIA amplitude observed is primarily due to CoPi species oxidized by $BiVO_4$ holes.

The key conclusion from the analysis shown in **Figure 5a** is that the onset of electrochemical water oxidation by CoPi appears at Co^{III} density of $> 1\times10^{17}$ cm^{-2},

approximately three fold higher than density of Co^{III} measured in our CoPi-modified $BiVO_4$ under conditions of photoelectrochemical water oxidation (3.2×10^{16} cm^{-2}). At the density of 3.2×10^{16} cm^{-2} Co^{III}, the corresponding electrochemical water oxidation current on CoPi/FTO is negligible ($\leq$ 100 μA cm^{-2}), $\leq$ 5 % of the observed photocurrent. This demonstrates that the magnitude of CoPi oxidation measured for the CoPi-$BiVO_4$ photoanodes studied herein under conditions of photoelectrochemical water oxidation is not sufficient to drive significant water oxidation from the CoPi layer alone. This point is further illustrated in **Figure 5b**, which overlays the measured photocurrent amplitude for CoPi-$BiVO_4$ as a function of excitation light intensity at 1.7 V_{RHE} (black line) with the calculated contribution to this water oxidation current from the CoPi layer alone (red line). The calculated CoPi water oxidation current was determined by taking the steady-state PIA amplitude of CoPi-modified $BiVO_4$ (*e.g.* from **Figure 3a**) to yield a Co^{III} density, and then reading off the current that this Co^{III} density corresponds to from **Figure 5a**. It is clear that the calculated photocurrent for water oxidation *via* CoPi on $BiVO_4$ during PIA measurements is negligible compared to the actual photocurrent measured, for all light intensities studied. This demonstrates that whilst the CoPi on $BiVO_4$ is indeed partially oxidized from Co^{II} to Co^{III}, the degree of oxidation is not sufficient to drive significant water oxidation via CoPi. As such, we conclude that photoelectrochemical water oxidation by CoPi-modified $BiVO_4$, as measured at the strong anodic potentials employed herein, primarily results from the direct oxidation of water by $BiVO_4$ holes, rather than from catalytic water oxidation *via* oxidized CoPi.

We now turn to a model illustrating the key processes driving water oxidation on the CoPi-modified $BiVO_4$ photoanodes studied herein, as illustrated in **Scheme 1**. The evidence for the timescales of the processes illustrated in this figure is discussed below. We note that we use timescales rather than rate constants in this model, as some of these processes do not exhibit first order kinetics, complicating the use of rate constants. This model is only concerned with the fate of $BiVO_4$ holes transferred to the $BiVO_4$ surface under strong anodic potential, and so

excludes both bulk recombination and back electron/hole recombination with these surface holes.

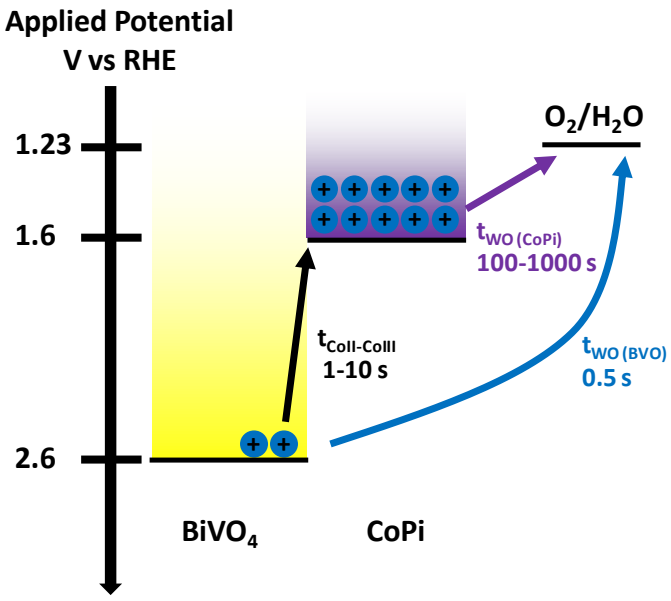

Scheme 1. Schematic representation of the kinetics of hole transfer at the $BiVO_4$ surface, based on the results discussed herein. All charge transfer times are defined the text.

Concerning the timescale of water oxidation by CoPi, Surendranath *et al.* have reported that the turnover frequency of CoPi water oxidation is 2×10^{-3} s^{-1}, or ~1000 s per turnover, defined as $t_{WO(CoPi)}$ per active site.[7] Similarly, Klingan *et al.* also reported that the turnover frequency of CoPi water oxidation varies between 1×10^{-2} s^{-1} and 1×10^{-3} s^{-1} for a 100 nm thick CoPi electrode.[8] We note that such numbers depend on measurement of 'active site' density, and are complicated by the onset behavior illustrated in **Figure 5** above. However, they are indicative that water oxidation on CoPi is kinetically rather slow, as illustrated in **Scheme 1**, with high electrochemical current densities deriving from the large density of Co active sites and high porosity of CoPi.[7]

Concerning water oxidation by photogenerated $BiVO_4$ holes, studies of unmodified $BiVO_4$ indicate that this occurs on timescales of 100 ms–1 s.[5e, 12c] We assume for simplicity that the timescale of this water oxidation is not impacted by a CoPi overlayer. We note that these data,

coupled together, highlight water oxidation on CoPi is ~1000 times slower than on $BiVO_4$. This is consistent with our conclusion of negligible (≤ 5%) water oxidation from CoPi on our CoPi-modified $BiVO_4$ films, even though the density of accumulated of Co^{III} species is ~100 greater than the density of $BiVO_4$ holes on an unmodified $BiVO_4$ photoanode. The faster water oxidation kinetics on $BiVO_4$ are most probably due to the larger driving force for water oxidation from the $BiVO_4$ valence band ($BiVO_4$ valence band edge at 2.6 V_{RHE} compared to the Co^{III}/Co^{II} redox potential of 1.55 V_{RHE}).

Our observation that water oxidation on CoPi-modified $BiVO_4$ primarily occurs via $BiVO_4$ holes indicates that hole transfer from $BiVO_4$ to CoPi must be slow relative to this water oxidation process. Taking the Co^{III} density measured under our conditions of photoelectrochemical water oxidation (3.2×10^{16} cm^{-2}), and using an oxidized cobalt lifetime for water oxidation of 100 s (from the discussion above), we conclude that a flux of holes to the CoPi layer of 3.2×10^{14} s^{-1} cm^{-2} would be required to accumulate this Co^{III} density. This corresponds to approximately 3 % of the measured photocurrent density (2 mA cm^{-2} or 1.3×10^{16} holes s^{-1} cm^{-2}), consistent with our conclusion above that ≤ 5 % the photocurrent derives from oxidized CoPi. This conclusion indicates a timescale for hole transfer from $BiVO_4$ to CoPi of 1–10 s, as indicated in **Scheme 1** (*i.e.* ~20 fold slower than direct water oxidation on $BiVO_4$). We note that this hole transfer is thermodynamically strongly downhill. As such our conclusion that this transfer is kinetically slow indicates there may be a barrier or incomplete physical contact between the $BiVO_4$ and CoPi layers. We note that following light turnoff, the PIA signal assigned to Co^{III} states decays on a ~1 s timescale. This appears to be too fast to correspond to water oxidation. Rather it is more probably associated with recombination between these accumulated Co^{III} states and bulk $BiVO_4$ electrons. This conclusion is supported by the observation of a significant reverse (negative) current spike following light turnoff in **Figure 3b**. The relatively fast timescale of this recombination, even

under strong anodic bias, may be associated with the high density of Co^{III} states accumulated in the CoPi layer.

The schematic illustrated in **Scheme 1** is only intended to be an indication of the timescales of the key processes, rather than a formal kinetic model, which is beyond the scope of this study. However it does illustrate the critical role of kinetics in determining the function, or in this case the lack of catalytic function, of an electrocatalyst deposited on a photoanode surface. We conclude that even though the CoPi is oxidized during photoelectrochemical water oxidation by CoPi-modified $BiVO_4$ photoanodes, this catalyst oxidation is not the origin of the enhanced photocurrent. We have reported previously that CoPi deposition results in significant reduction in recombination losses in the $BiVO_4$, and specifically retards back electron/hole or 'surface' recombination.[5e] We have moreover previously shown that the magnitude of this retardation of reduction losses is alone sufficient to explain the improved performance of CoPi-modified $BiVO_4$, without requiring any direct impact of the electrocatalytic function of CoPi. Our study herein provides strong evidence that this reduction in recombination losses, rather than an improvement (acceleration) in water oxidation catalysis, is indeed the origin of the improved water oxidation by $BiVO_4$ following CoPi deposition.

The analysis illustrated in Scheme 1 is of course only for the photoelectrodes studied herein, and may be dependent upon the details of $BiVO_4$ or CoPi deposition. Whilst a full analysis of these contributions is beyond the scope of this study, we did undertake an analogous study using thinner (~10 nm CoPi) layers, as detailed in the supporting information (**Figure S8**). Broadly similar data were obtained, again indicating that water oxidation is primarily driven directly from $BiVO_4$ holes. We note that in the limit of very thick CoPi layers, water oxidation *via* such CoPi layers is likely to contribute increasingly to the overall water oxidation flux, as has been proposed by Carroll *et al.*,[10a] although in our studies, such thicker CoPi layers resulted in an overall loss of photoanode performance.

The results from both thin and thick CoPi-modified $BiVO_4$ photoanodes suggest that the charge transfer of holes from $BiVO_4$ to CoPi is not efficient, as these hole transfer kinetics are slower than direct water oxidation by $BiVO_4$ holes, despite the strong thermodynamic driving force from the valence band edge of $BiVO_4$ (2.6 V_{RHE}) to the Co^{III}/Co^{II} redox potential (1.55 V_{RHE}). As a result, water oxidation occurs primarily *via* holes accumulated at the $BiVO_4$ surface, rather than *via* CoPi. Consequently, our current research is focusing on optimization of the CoPi/$BiVO_4$ interface and using a "faster" catalyst as the overlayer on $BiVO_4$, for example FeOOH or NiOOH.

4. Conclusion

In this paper, we have focused on the catalytic function of CoPi on $BiVO_4$ photoanodes during photo-assisted water oxidation using photo-induced absorption spectroscopy and spectroelectrochemical methods under quasi steady-state conditions. Holes photo-generated in $BiVO_4$ are observed to oxidize CoPi from Co^{II} to Co^{III} on CoPi-modified $BiVO_4$ under conditions of photoelectrochemical water oxidation, resulting in a steady state accumulation of ~3.2 x 10^{16} Co^{III} cm^{-2}. However studies of dark water oxidation by CoPi/FTO demonstrate a strongly non-linear dependence of electrocatalytic water oxidation flux upon Co^{III} density, with an onset at ~1×10^{17} Co^{III} cm^{-2}. As such we conclude that under conditions of photoelectrochemical water oxidation on the CoPi-modified $BiVO_4$ photoanodes studied herein, CoPi oxidation does not contribute significantly to the overall water oxidation current ($\leq$ 5 %). Rather water oxidation on these photoanodes occurs primarily via holes at the $BiVO_4$ surface, with the efficiency of this process being enhanced by CoPi deposition due its ability to retard electron/hole recombination within the $BiVO_4$ photoanode. Our results indicate that efficient electrocatalyst function on such photoanodes will require sufficiently rapid hole transfer from the semiconductor to the catalyst to be competitive with water oxidation by

holes in the semiconductor. In addition, careful consideration should be given to the relative kinetics of water by the semiconductor and catalyst.

5. Experimental Section

Bismuth vanadate Photoanodes: All chemicals used in this study were purchased from Sigma-Aldrich with the highest purity, unless otherwise stated. Undoped (not intentionally doped) $BiVO_4$ photoanodes were fabricated using a modified metal-organic deposition with spincoating, as described previously.[12c, 23] The film thickness is approximately 450 nm and the film is dense and flat, as reported previously.[12c]

Cobalt Phosphate Deposition on $BiVO_4$ and FTO substrate: Cobalt phosphate on FTO[6] and $BiVO_4$[3b, 5e] was deposited using the method previously described. Briefly, photo-assisted electrodeposition was used to deposit CoPi on the surface of the $BiVO_4$ photoanodes at 1.2 V_{RHE} applied potential. The deposition time was controlled to be 1 minute and 10 minutes for thin and thick CoPi overlayers, respectively, under illumination (75 W Xenon lamp, ~ 100 mW cm^{-2}). The electrolyte was prepared with 0.5 mM cobalt nitrite ($Co(NO_3)_2$) with 0.1 M potassium phosphate buffer (0.1 M K_2HPH_4 and KH_2PO_4, pH 6.7). As reported previously, a 10 minutes deposition time under these conditions (corresponding to 1.2 C cm^{-2} of charges passing through the electrode) results in an approximately 100 nm thick CoPi film.[5e] This deposition time was found to give optimum photoanode performance for the photoanodes employed herein. Electrodeposition of CoPi on FTO substrates was carried out using the same method, but without illumination. The FTO was immersed in the KPi buffer containing $Co(NO_3)_2$ under 1.9 V_{RHE} applied potential for 1 min (charges passing through the electrode: 0.12 C cm^{-2}, total cobalt density: 8.6×10^{17} cm^{-2}) and 10 minutes (1.2 C cm^{-2}, 8.6×10^{18} cm^{-2}) for 10 nm and 100 nm thick CoPi layers, respectively.

Physical Characterization : Scanning electron microscopy (SEM) measurements were carried out using a ZEISS FEG-SEM microscope (LEO 1525 equipped with GEMINI field emission column) with acceleration voltage of 5 kV. Samples prepared for SEM measurements were coated with 10 nm chromium particles to enhance sample conductivity.

X-ray diffraction (XRD) was conducted with a modified Bruker-Axs D8 diffractometer with parallel beam optics equipped with a PSD Linx-Eye silicon strip detector. A Cu source generated X-rays; with Cu Kα1 and Cu Kα2 radiation of $\lambda = 1.54056$ and 1.54439 Å respectively, emitted with an intensity ratio of 2:1 at an applied potential of 40 kV and 30 mA of current. The incident beam was kept at 1° and the angular range of the patterns collected was $10° < 2\theta < 66°$ with a step size of 0.025°. Patterns were fitted to a Le Bail refined model using the GSAS-EXPGUI software suite.[24]

X-ray photoelectron spectroscopy (XPS) was carried out using a Thermo K-Alpha spectrometer using monochromated Al Kα radiation. Scans were collected over the 0–1400 eV binding energy range with 1 eV resolution and a pass energy of 200 eV. An Ar-ion gun was used to etch the surface layers of samples to record a depth profile. A sputtering time of 5 s per level was used for a total of 5 levels. Peaks were modelled using CasaXPS.[25] Peak positions were adjusted to adventitious graphite (284.5 eV) and areas were converted using the appropriate sensitivity factors[26] to determine the concentration of each state.

Photoelectrochemical Measurements: Photoelectrochemical characterization of $BiVO_4$ photoanodes was carried out in a home-made cell with quartz windows in front and back of the cell. The electrolyte was 0.1 M potassium phosphate buffer (0.1 M K_2HPH_4 and KH_2PO_4, pH 6.7). An Autolab potentostat (PGSTAT 12) was employed to control the applied potential, and the current data were recorded using the NOVA software. A three-electrode configuration was employed which consisted of the $BiVO_4$ working electrode, an Ag/AgCl/sat'd KCl reference electrode (0.197 V_{NHE} at 298K; Metrohm) and a platinum mesh counter electrode.

All applied potentials were recorded *versus* the reference electrode and then converted to be *versus* the reversible hydrogen electrode using the Nernst equation,

$$E_{RHE}(V) = E_{Ag/AgCl}(V) + 0.0591 \times pH + E^{0}_{Ag/AgCl} \quad (1)$$

where E_{RHE} is the applied potential *versus* the reversible hydrogen electrode (RHE); $E_{Ag/AgCl}$ is the applied potential *versus* the Ag/AgCl/sat'd KCl reference electrode; $E^{0}_{Ag/AgCl}$ is the standard potential of the Ag/AgCl reference electrode.

The illumination light used for PEC measurements was generated from 365 nm LEDs (LZ1-10U600, LedEngin. Inc.). All measurements were conducted using back-side illumination (FTO-$BiVO_4$ side) to avoid parasitic absorption by CoPi overlayers. The light intensity at 365 nm was measured using a calibrated optical powermeter (PM 100, Thorlabs) with a power sensor (S120UV, Thorlabs), and is quoted in terms of its intensity relative to AM 1.5 intensity[27] between 280 nm and 500 nm based on the photon flux arriving at the sample surface (see Supporting Information).

Photo-Induced Absorption (PIA) Spectroscopy: The photo-induced absorption spectroscopy employed herein is a transiet pump-probe technique; the equipment setup has been reported previously.[20] The applied potential was controlled using a potentiostat (Ministat 251, Sycopel Scientific Ltd). Long-pulsed (~seconds) LED light was used to excite electrons across the band gap in the photoanode. The frequency of light on/off was controlled by a frequency generator (TG300, Thurlby Thandar Instruments). For the PIA measurements of unmodified $BiVO_4$, the excitation duration was 5 s, followed by 5 s in the dark, by which time the photocurrent and optical signals had reached approximately steady-state. For the CoPi-modified $BiVO_4$, the excitation time was 8.5 s then the sample was kept in dark for 20 s to allow excited species to return to ground state before the next excitation. The dynamics of photogenerated charges were monitored by measuring the difference in absorbance (ΔOD) of

the sample before and after the LED light pulse, as a function of time. Monochromatic light from a tungsten lamp is employed as the probe beam; the transmittance of photons through the sample is monitored using a Si photodiode detector (Hamamatsu S3071). Raw data are collected using a DAQ card (National Instruments NI USB-6211) for the optical data and an oscilloscope (Tektronics TDS 2012c) for transient photocurrent data.

The photocurrent response was monitored by recording the potential response across a resistor (9.8 kΩ) set between the working and counter electrodes. This potential was converted to current using Ohm's law. The photocurrent and absorption responses shown are the results of averaging 30-70 measurements.

Spectroelectrochemistry: Spectroelectrochemical (SEC) measurements were conducted to measure the UV-Vis absorption spectra of CoPi/FTO in a PEC cell under applied potential, using a UV-Vis spectrometer (Lambda 25, Perkin Elmer). The applied potentials were controlled using an Autolab potentiostat (PGSTAT 12). All SEC spectra were measured under steady-state conditions; each potential was applied for 60 s before the UV-Vis measurement. SEC spectra were obtained by subtracting the UV-Vis spectrum at the open-circuit condition, *i.e*. an isolated CoPi/FTO film in the electrolyte without connection to the potentiostat, from each UV-Vis spectrum under applied potential.

$$\Delta OD_{SEC}(V) = OD(V) - OD_{OC} \quad (2)$$

where $\Delta OD_{SEC}(V)$ is the SEC amplitude; $OD(V)$ is the measured absorption signal from 500 nm to 900 nm under a given applied potential; OD_{OC} is the absorption signal from the same wavelength range measured at open circuit without connection to the potentiostat. The current after 60 s at each potential was recorded during the SEC measurements.

Supporting Information

Supporting Information is available from the Wiley Online Library or from the author.

Acknowledgements

Y.M., A.K., S.R.P., F.L.F. and J.R.D. thank the European Research Council (project Intersolar 291482) for funding. A.K. thanks the Ramsay Memorial Fellowships Trust. F.L.F. thanks the Swiss National Science Foundation (project: 140709). The authors also thank Dr Xiaoe Li for help with SEM measurements.

Received: ((will be filled in by the editorial staff))
Revised: ((will be filled in by the editorial staff))
Published online: ((will be filled in by the editorial staff))

[1] M. Gratzel, *Nature* **2001**, *414*, 338.
[2] a) A. J. Cowan, J. R. Durrant, *Chem. Soc. Rev.* **2013**, *42*, 2281; b) L. Peter, *J. Solid State Electrochem.* **2013**, *17*, 315.
[3] a) T. W. Kim, K.-S. Choi, *Science* **2014**, *343*, 990; b) D. K. Zhong, S. Choi, D. R. Gamelin, *J. Am. Chem. Soc.* **2011**, *133*, 18370; c) F. F. Abdi, L. Han, A. H. M. Smets, M. Zeman, B. Dam, R. van de Krol, *Nat. Commun.* **2013**, *4*, 2195.
[4] a) B. Klahr, S. Gimenez, F. Fabregat-Santiago, J. Bisquert, T. W. Hamann, *J. Am. Chem. Soc.* **2012**, *134*, 16693; b) D. E. Wang, R. G. Li, J. Zhu, J. Y. Shi, J. F. Han, X. Zong, C. Li, *J. Phys. Chem. C* **2012**, *116*, 5082.
[5] a) C. Y. Cummings, F. Marken, L. M. Peter, A. A. Tahir, K. G. U. Wijayantha, *Chem. Commun.* **2012**, *48*, 2027; b) M. Barroso, S. R. Pendlebury, A. J. Cowan, J. R. Durrant, *Chem. Sci.* **2013**, *4*, 2724; c) M. Barroso, C. A. Mesa, S. R. Pendlebury, A. J. Cowan, T. Hisatomi, K. Sivula, M. Grätzel, D. R. Klug, J. R. Durrant, *P Natl Acad Sci USA* **2012**, *109*, 15640; d) M. Barroso, A. J. Cowan, S. R. Pendlebury, M. Grätzel, D. R. Klug, J. R. Durrant, *J. Am. Chem. Soc.* **2011**, *133*, 14868; e) Y. Ma, F. Le Formal, A. Kafizas, S. R. Pendlebury, J. R. Durrant, *J. Mater. Chem. A* **2015**, *3*, 20649; f) F. Le Formal, K. Sivula, M. Grätzel, *J. Phys. Chem. C* **2012**, *116*, 26707.
[6] M. W. Kanan, D. G. Nocera, *Science* **2008**, *321*, 1072.
[7] Y. Surendranath, M. W. Kanan, D. G. Nocera, *J. Am. Chem. Soc.* **2010**, *132*, 16501.
[8] K. Klingan, F. Ringleb, I. Zaharieva, J. Heidkamp, P. Chernev, D. Gonzalez-Flores, M. Risch, A. Fischer, H. Dau, *ChemSusChem* **2014**, *7*, 1301.
[9] a) F. F. Abdi, N. Firet, R. van de Krol, *ChemCatChem* **2013**, *5*, 490; b) F. F. Abdi, R. van de Krol, *J. Phys. Chem. C* **2012**, *116*, 9398.
[10] a) G. M. Carroll, D. K. Zhong, D. R. Gamelin, *Energy Environ. Sci.* **2015**, *8*, 577; b) D. K. Zhong, M. Cornuz, K. Sivula, M. Gratzel, D. R. Gamelin, *Energy Environ. Sci.* **2011**, *4*, 1759.
[11] G. M. Carroll, D. R. Gamelin, *Journal of Materials Chemistry A* **2016**, 10.1039/C5TA06978E.
[12] a) C. Y. Cummings, F. Marken, L. M. Peter, K. G. Upul Wijayantha, A. A. Tahir, *J. Am. Chem. Soc.* **2011**, *134*, 1228; b) F. Le Formal, S. R. Pendlebury, M. Cornuz, S. D. Tilley, M. Grätzel, J. R. Durrant, *J. Am. Chem. Soc.* **2014**, *136*, 2564; c) Y. Ma, S. R. Pendlebury, A. Reynal, F. Le Formal, J. R. Durrant, *Chem. Sci.* **2014**, *5*, 2964; d) S. R. Pendlebury, X. Wang, F. Le Formal, M. Cornuz, A. Kafizas, S. D. Tilley, M. Grätzel, J. R. Durrant, *J. Am. Chem.*

Soc. **2014**, *136*, 9854; e) S. R. Pendlebury, A. J. Cowan, M. Barroso, K. Sivula, J. Ye, M. Gratzel, D. R. Klug, J. Tang, J. R. Durrant, *Energy Environ. Sci.* **2012**, *5*, 6304; f) F. M. Pesci, A. J. Cowan, B. D. Alexander, J. R. Durrant, D. R. Klug, *J. Phys. Chem. Lett.* **2011**, *2*, 1900; g) S. R. Pendlebury, M. Barroso, A. J. Cowan, K. Sivula, J. W. Tang, M. Gratzel, D. Klug, J. R. Durrant, *Chem. Commun.* **2011**, *47*, 716; h) A. J. Cowan, C. J. Barnett, S. R. Pendlebury, M. Barroso, K. Sivula, M. Gratzel, J. R. Durrant, D. R. Klug, *J. Am. Chem. Soc.* **2011**, *133*, 10134; i) A. J. Cowan, J. W. Tang, W. H. Leng, J. R. Durrant, D. R. Klug, *J. Phys. Chem. C* **2010**, *114*, 4208; j) J. W. Tang, J. R. Durrant, D. R. Klug, *J. Am. Chem. Soc.* **2008**, *130*, 13885.

[13] L. Trotochaud, J. K. Ranney, K. N. Williams, S. W. Boettcher, *J. Am. Chem. Soc.* **2012**, *134*, 17253.

[14] a) B. J. Tan, K. J. Klabunde, P. M. A. Sherwood, *J. Am. Chem. Soc.* **1991**, *113*, 855; b) N. S. McIntyre, M. G. Cook, *Analytical Chemistry* **1975**, *47*, 2208.

[15] L. Fu, H. Yu, C. Zhang, Z. Shao, B. Yi, *Electrochim. Acta* **2014**, *136*, 363.

[16] T. P. Debies, J. W. Rabalais, *Chemical Physics* **1977**, *20*, 277.

[17] R. Larsson, B. Folkesson, B. Folkesson, *Chem. Scr.* **1973**, *3*, 88.

[18] A. Kafizas, N. Noor, P. Carmichael, D. O. Scanlon, C. J. Carmalt, I. P. Parkin, *Advanced Functional Materials* **2014**, *24*, 1758.

[19] a) J. Ravensbergen, F. F. Abdi, J. H. van Santen, R. N. Frese, B. Dam, R. van de Krol, J. T. M. Kennis, *J. Phys. Chem. C* **2014**, *118*, 27793; b) Z. Huang, Y. Lin, X. Xiang, W. Rodriguez-Cordoba, K. J. McDonald, K. S. Hagen, K.-S. Choi, B. S. Brunschwig, D. G. Musaev, C. L. Hill, D. Wang, T. Lian, *Energy Environ. Sci.* **2012**, *5*, 8923; c) T. Yoshihara, R. Katoh, A. Furube, Y. Tamaki, M. Murai, K. Hara, S. Murata, H. Arakawa, M. Tachiya, *J. Phys. Chem. B* **2004**, *108*, 3817.

[20] F. Le Formal, E. Pastor, S. D. Tilley, C. A. Mesa, S. R. Pendlebury, M. Gratzel, J. R. Durrant, *J Am Chem Soc* **2015**, *137*, 6629.

[21] B. J. Trzesniewski, W. A. Smith, *Journal of Materials Chemistry A* **2016**, 10.1039/C5TA04716A.

[22] a) H. S. Ahn, A. J. Bard, *J. Am. Chem. Soc.* **2015**, *137*, 612; b) J. G. McAlpin, Y. Surendranath, M. Dincă, T. A. Stich, S. A. Stoian, W. H. Casey, D. G. Nocera, R. D. Britt, *Journal of the American Chemical Society* **2010**, *132*, 6882.

[23] K. Sayama, A. Nomura, T. Arai, T. Sugita, R. Abe, M. Yanagida, T. Oi, Y. Iwasaki, Y. Abe, H. Sugihara, *J. Phys. Chem. B* **2006**, *110*, 11352.

[24] B. Toby, *Journal of Applied Crystallography* **2001**, *34*, 210.

[25] Casa Software Ltd http://www.casaxps.com/ (accessed Dec 13, 2014).

[26] D. Briggs, M. P. Seah, *Practical Surface Analysis by Auger and X-ray Photoelectron Spectroscopy*, John Wiley and Sons, Chichester.

[27] Reference Solar Spectral Irradiance: Air Mass 1.5. NREL. ASTMG-173 package. http://rredc.nrel.gov/solar/spectra/am1.5/

Photo-induced absorption spectroscopy is employed to investigate charge carrier dynamics in CoPi-modified $BiVO_4$ photoanodes for water oxidation under simulated working condition. The quantity of oxidized CoPi by $BiVO_4$ holes is found to be low and incapable of driving efficient water oxidation. Therefore, almost no catalytic function from the CoPi layer is present in CoPi-modified $BiVO_4$ under working photoelectrochemical conditions.

Keyword: cobalt phosphate, bismuth vanadate, water oxidation, photoelectrochemistry, kinetics

Yimeng Ma, Andreas Kafizas, Stephanie R. Pendlebury, Florian Le Formal and James R. Durrant*

Photo-Induced Absorption Spectroscopy of CoPi on $BiVO_4$: The Function of CoPi During Water Oxidation

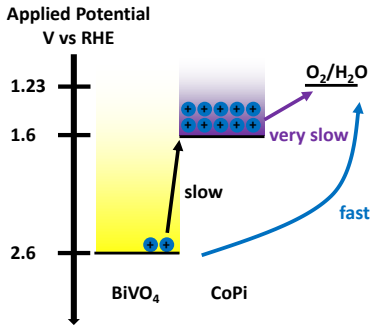

Supporting Information

Photo-Induced Absorption Spectroscopy of CoPi on $BiVO_4$: The Function of CoPi During Water Oxidation

*Yimeng Ma, Andreas Kafizas, Stephanie R. Pendlebury, Florian Le Formal and James R. Durrant**

Calculation of the LED intensity compared to AM 1.5 radiation

For PIA and TPC measurements, the excitation source was one / two 365 nm LEDs depending on the intensity required. The intensity of the LED illumination has been converted to the ratio compared with AM 1.5 intensity in terms of the number of photons.

The single photon energy is calculated using Equation S1:

$$E(\lambda) = h \times \frac{c}{\lambda} \quad \text{(S1)}$$

where $E(\lambda)$ is the photon energy (J), h is the Planck's constant (6.626×10^{-34} J s), C is the speed of light (3×10^{8} m s^{-1}) and λ is the photon wavelength (m).

The solar photon flux is then calculated from Equation S2:

$$flux(\lambda) = \frac{P(\lambda)}{E(\lambda)} \quad \text{(S2)}$$

where $flux(\lambda)$ is the solar photon flux (m^{-2} s^{-1} nm^{-1}), and $P(\lambda)$ is the solar power flux (W m^{-2} nm^{-1}). The AM 1.5 solar power flux data were obtained from NREL.[1]

Integration of the solar photon flux gives the photon flux (m^{-2} s^{-1}) across the wavelength selected. For $BiVO_4$, the absorption edge is 500 nm, therefore, the photon flux under 500 nm is obtained from Equation S3:

$$flux(\lambda < 500nm) = \int_{280nm}^{500nm} flux(\lambda) d\lambda = 4\times10^{20}\ m^{-2}s^{-1} \quad \text{(S3)}$$

where 500 nm is the $BiVO_4$ absorption edge; 280 nm is the lower limit of AM 1.5 spectrum. The integration yields the photon flux of 4×10^{20} m^{-2} s^{-1} at the $BiVO_4$ surface under AM 1.5 condition.

The light power was measured by an optical power meter (PM 100, Thorlabs) with a power sensor (S120UV, Thorlabs) at 365 nm, and then converted to the photon flux using Equation S4:

$$flux(365nm, LED) = \frac{P(365nm)}{E(365nm)} \quad \text{(S4)}$$

The rate of LED light vs AM 1.5 (*rate (%)*) is obtained by measuring the power at 365 nm and converted using Equation S5,

$$rate(\%) = \frac{flux(365nm, LED)}{4 \times 10^{20} m^{-2} s^{-1}} \times 100\% \quad \text{(S5)}$$

SEM and XRD of CoPi/FTO

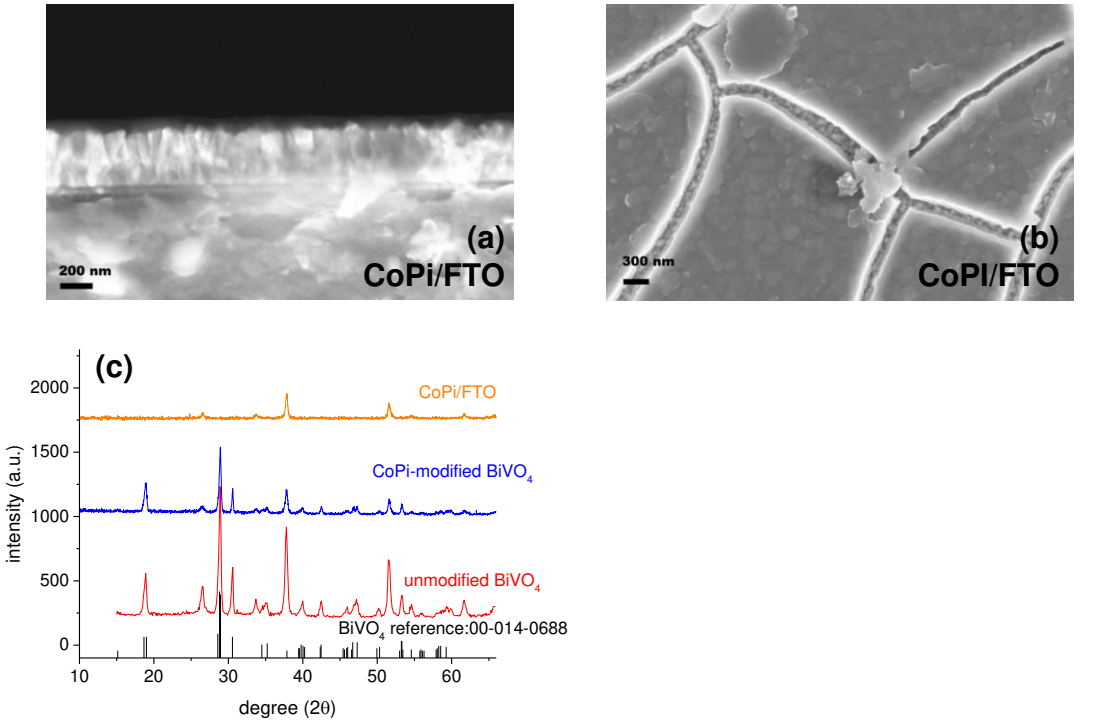

Figure S1. (a) Cross-sectional SEM image of CoPi/FTO electrodes. (b) Top-view SEM image of CoPi/FTO electrode. (c) XRD patterns of CoPi/FTO (orange); CoPi-modified $BiVO_4$ photoanode (blue); unmodified $BiVO_4$ photoanode (red). XRD reference for unmodified $BiVO_4$ (black bars): 00-014-0688.

XPS of CoPi-modified $BiVO_4$ and CoPi/FTO electrodes

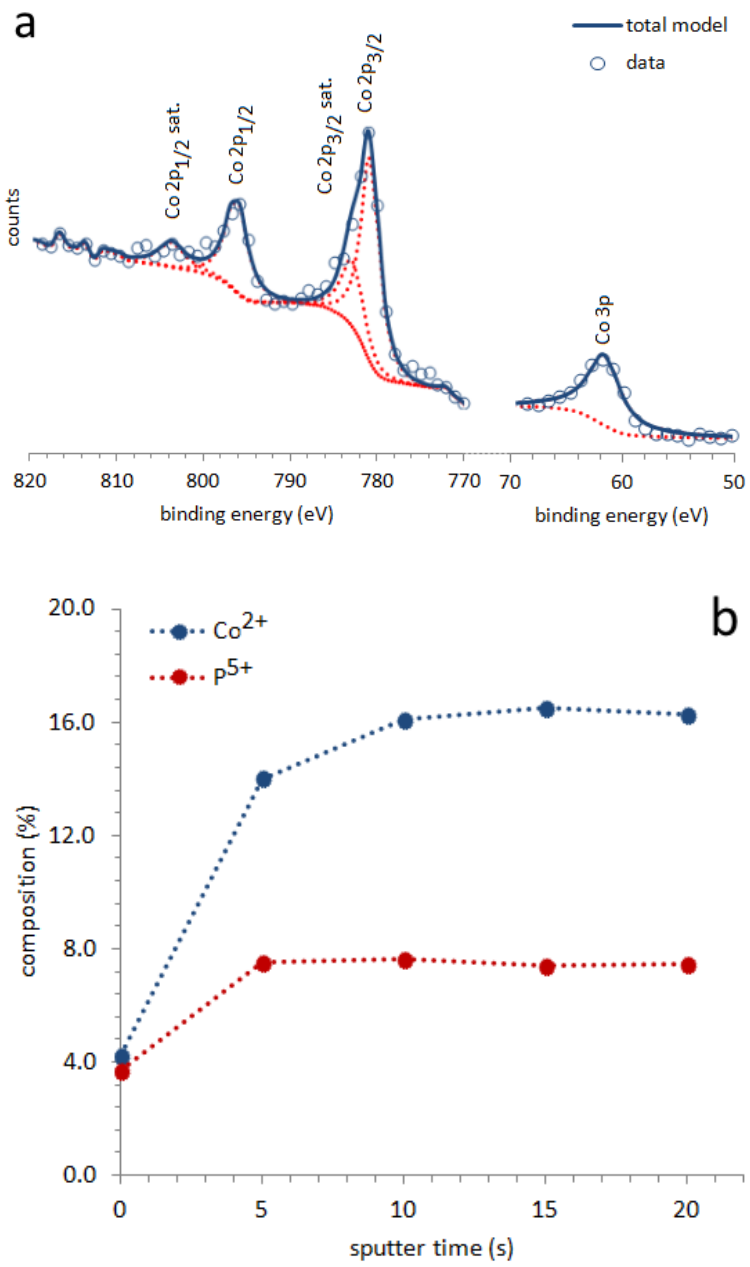

Figure S2. (a) XPS spectra of the Co_{2p} (820 – 770 eV) and Co_{3p} (70 – 50 eV) binding energy regions shown alongside the deconvolution of each Co state and satellite states for CoPi grown on FTO. (b) The composition of Co^{2+} and P^{5+} *versus* sputter time (s) for CoPi grown on FTO, as measured by XPS.

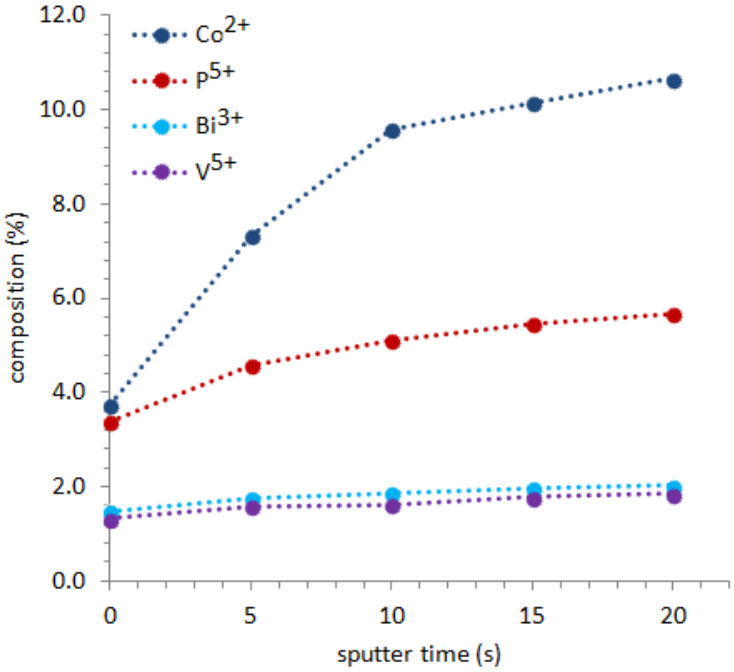

Figure S3. The composition of Co^{2+}, P^{5+}, Bi^{3+} and V^{5+} *versus* sputter time (s) for CoPi-modified $BiVO_4$, as measured by XPS.

Scan Rate Dependent of CoPi/FTO

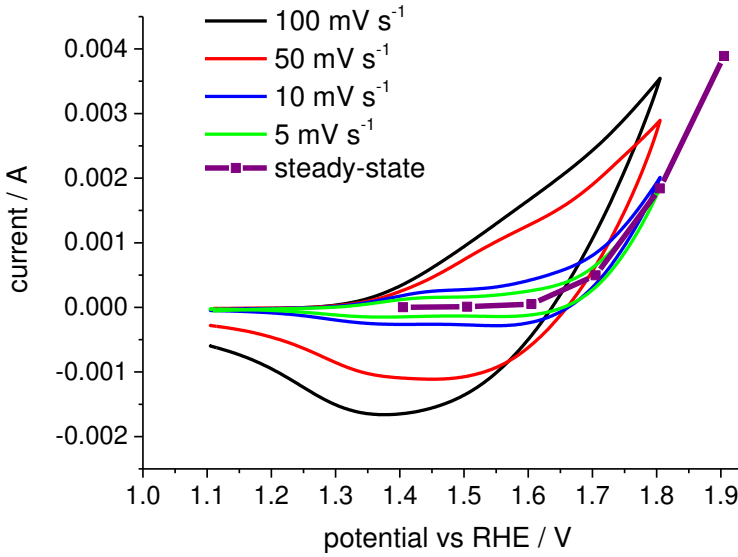

Figure S4. Cyclic voltammetry of a CoPi/FTO electrode from 1.1 V_{RHE} with different scan rate from 5 mV^{-1} to 100 mV s^{-1}, and the steady-state current measured as a function of applied potential (purple line and squares).

PIA Spectra of Unmodified $BiVO_4$ and CoPi-modified $BiVO_4$

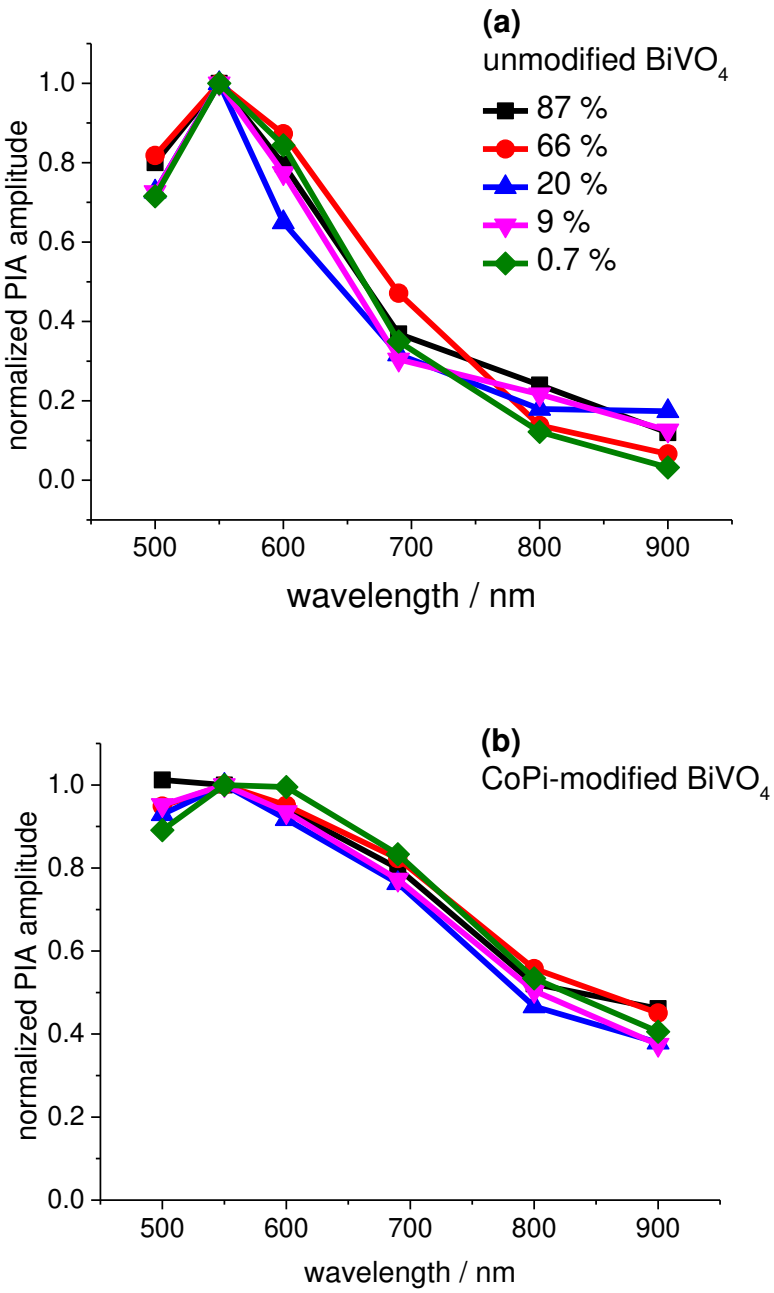

Figure S5. Normalized PIA spectra as a function of LED intensities: (a) unmodified $BiVO_4$ and (b) CoPi-modified $BiVO_4$. The LED intensities in (a) also applies to (b).

Determination of Extinction Coefficient of $BiVO_4$ Photogenerated Holes

The extinction coefficient of $BiVO_4$ photogenerated holes was determined using photo-induced absorption spectroscopy. Applying an electrode potential where there is back electron/hole recombination dominating the PIA amplitude, and no photocurrent is observed, the photocurrent response measured concurrently represents the amount of charges for back electron/hole recombination. Therefore, the extinction coefficient can be obtained using Bert-Lambert Law:

$$\Delta OD = \varepsilon_{h^+} \times P_s \quad \text{(S6)}$$

where ΔOD is the PIA amplitude of photogenerated holes in $BiVO_4$ for back electron/hole recombination; ε_{h+} is the extinction coefficient of photogenerated holes and p_s is the surface hole density.

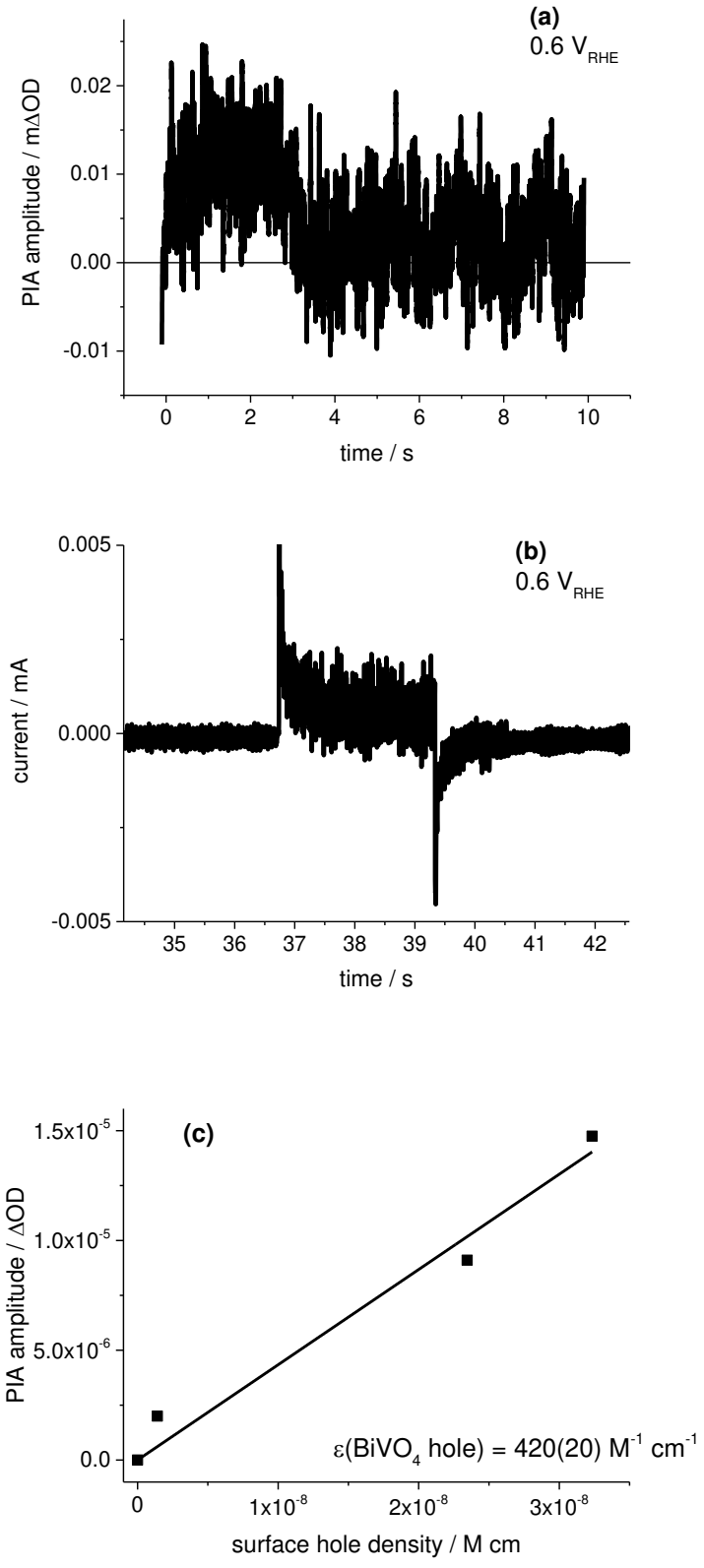

Figure S6. Determination of the extinction coefficient of $BiVO_4$ photogenerated holes. PIA amplitude (a) and TPC response (b) measured at 0.6 V_{RHE} at 87 % AM 1.5 light intensity. The

Beer-Lambert plot (c) indicates the extinction coefficient of BiVO4 photogenerated holes is $420 \pm 20\ M^{-1}\ cm^{-1}$.

Determination of Extinction Coefficient of Photo/Potential-induced Co^{III} Species

Spectroelectrochemical measurements of CoPi/FTO electrodes indicated that at applied potentials between 1.4 and 1.6 V_{RHE}, there was a potential-induced transient current in the beginning but no significant water oxidation current generated by the electrode at the steady state. However, the SEC spectra clearly showed there were charged species, as have been assigned to a non-Faradaic process to generate Co^{III} species. Therefore, the potential-induced charge in the current transients can be correlated with the optical SEC spectra. Using Beer-Lambert law, the extinction coefficient of this Co^{III} species can be obtained. The photo-induced Co^{III} species in CoPi-modified $BiVO_4$ photoanodes has also identified as the same species as the potential-induced species in SEC measurements.

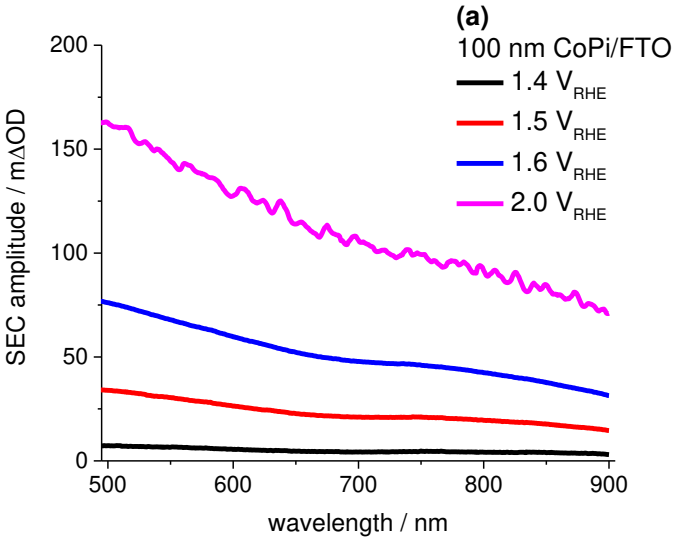
(a)
100 nm CoPi/FTO
1.4 V RHE
1.5 V RHE
1.6 V RHE
2.0 V RHE
SEC amplitude / mΔOD
wavelength / nm

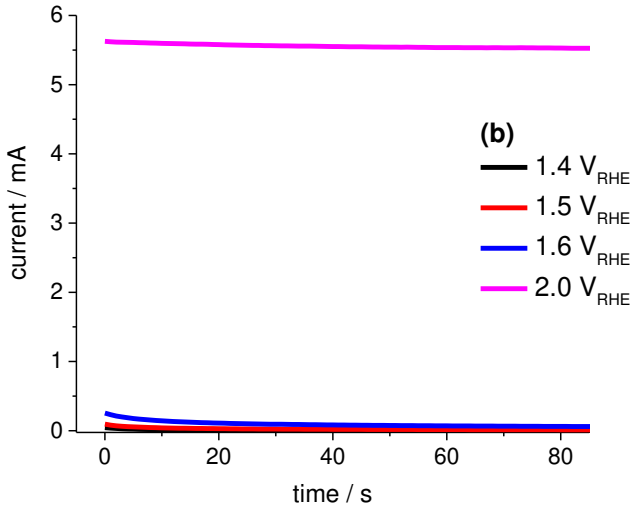
(b)
1.4 V RHE
1.5 V RHE
1.6 V RHE
2.0 V RHE
current / mA
time / s

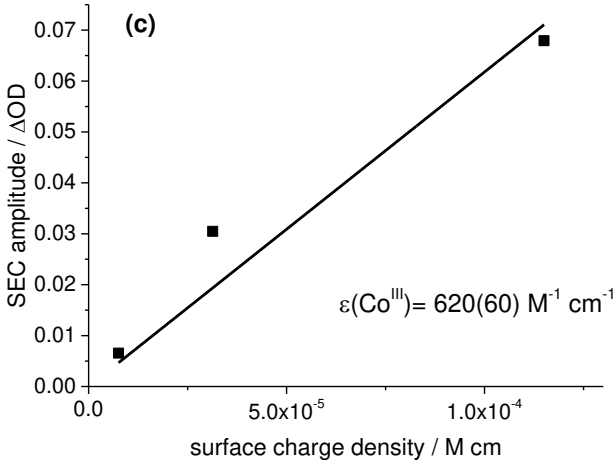
(c)
ε(Co III)= 620(60) M-1 cm-1
SEC amplitude / ΔOD
surface charge density / M cm

Figure S7. Determination of the extinction coefficient of potential-induced Co^{III} species using spectroelectrochemical methods. SEC amplitude (a) and chronoamperometric response (b) measured between 1.4 and 1.6 V_{RHE}, compared with the SEC results measured at 2.0 V_{RHE}. The Beer-Lambert plot (c) indicates the extinction coefficient of these charged Co^{III} is ~ 620 ± 60 M^{-1} cm^{-1}.

6. PIA and SEC Measurements of A Thin CoPi-modified $BiVO_4$ Photoanode

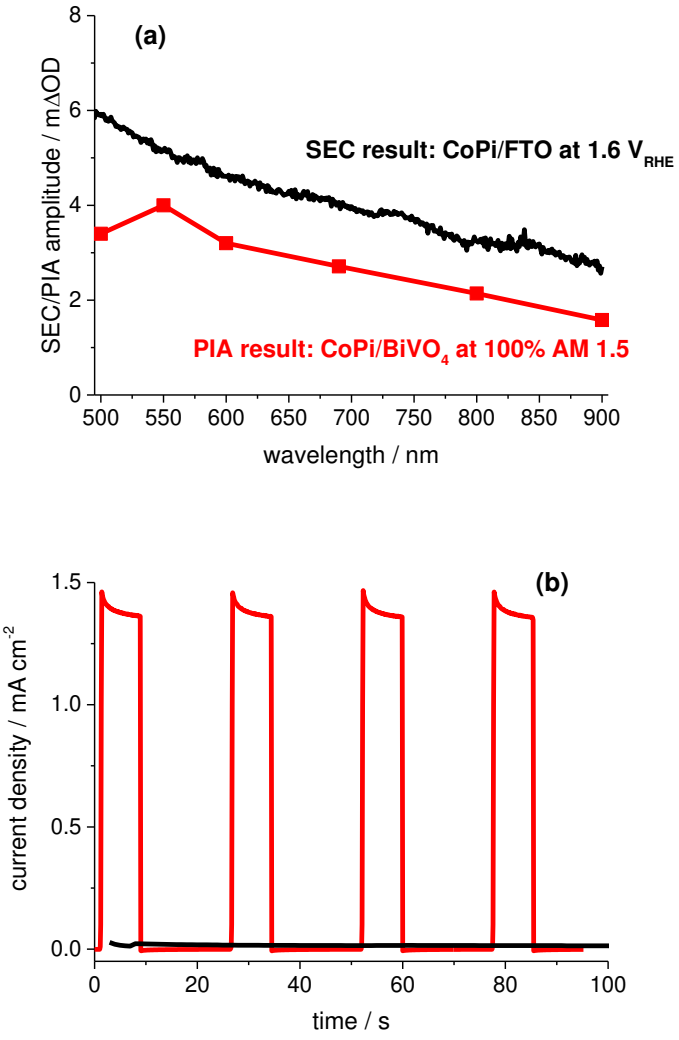

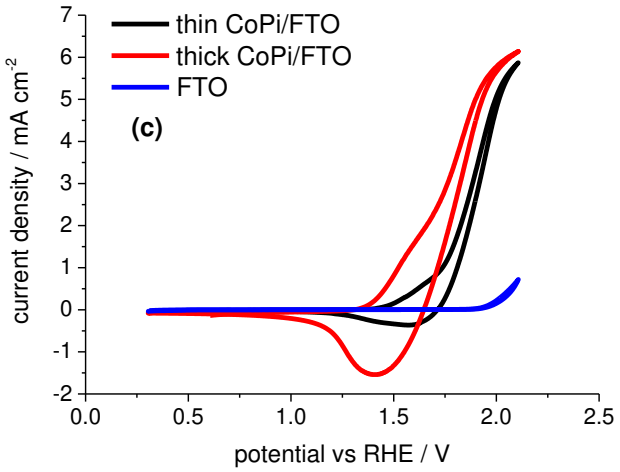

Figure S8. Comparison of optical absorption spectra (a) and current density of water oxidation (b) of photo-/potential-induced CoIII species in a thin CoPi-modified $BiVO_4$ photoanode (red) and a thin CoPi/FTO electrode (black). The color code in (b) matches with (a). The film thickness for both electrodes were estimated to be ca. 10 nm determined from the deposition time compared to that for 100 nm thick CoPi overlayers. (c) Comparison of CV results of 100 nm (red) and 10 nm (black) CoPi/FTO electrodes. Blue: bare FTO. Scan rate: 100 mV s^{-1}.

[1] Reference Solar Spectral Irradiance: Air Mass 1.5. NREL. ASTMG-173 package. http://rredc.nrel.gov/solar/spectra/am1.5/